

NJC

Accepted Manuscript



This is an *Accepted Manuscript*, which has been through the Royal Society of Chemistry peer review process and has been accepted for publication.

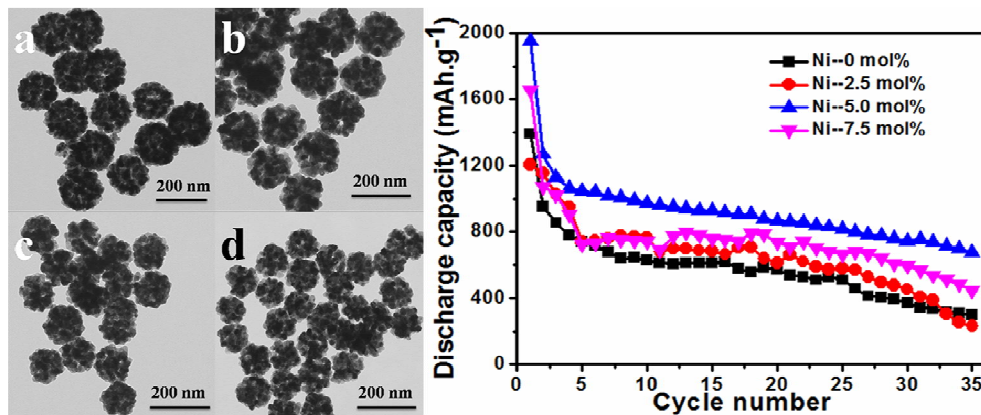
Accepted Manuscripts are published online shortly after acceptance, before technical editing, formatting and proof reading. Using this free service, authors can make their results available to the community, in citable form, before we publish the edited article. We will replace this *Accepted Manuscript* with the edited and formatted *Advance Article* as soon as it is available.

You can find more information about *Accepted Manuscripts* in the [Information for Authors](#).

Please note that technical editing may introduce minor changes to the text and/or graphics, which may alter content. The journal's standard [Terms & Conditions](#) and the [Ethical guidelines](#) still apply. In no event shall the Royal Society of Chemistry be held responsible for any errors or omissions in this *Accepted Manuscript* or any consequences arising from the use of any information it contains.

One step synthesis of Ni doped SnO₂ nanospheres with enhanced lithium ion storage performance

Xiaomin Ye, Wenjing Zhang, Qianjin Liu, Shuping Wang, Yanzhao Yang, Huiying Wei*



Ni doped SnO₂ nanospheres were prepared and exhibited excellent cycle performance and capacity retention.

* Corresponding author: Tel: +86-531-88365431; Fax: +86-531-88564464;

E-mail address: weihuiying@sdu.edu.cn

Cite this: DOI: 10.1039/c0xx00000x

www.rsc.org/xxxxxx

ARTICLE TYPE

One step synthesis of Ni-doped SnO₂ nanospheres with enhanced lithium ion storage performance

Xiaomin Ye,^a Wenjing Zhang,^a Qianjin Liu,^a Shuping Wang,^a YanzhaoYang^a and Huiying Wei^{*a}*Received (in XXX, XXX) Xth XXXXXXXXXX 20XX, Accepted Xth XXXXXXXXXX 20XX*

DOI: 10.1039/b000000x

In our work, Ni doped SnO₂ nanospheres have been synthesized via one step hydrothermal method using glucose as the soft template. Their structure and physicochemical properties were investigated using X-ray diffraction (XRD), a transmission electron microscope (TEM), a field-emission scanning electron microscope (FE-SEM) equipped with energy-dispersive X-ray spectroscopy (EDS), a high resolution transmission electron microscopy (HRTEM) and electrochemical methods. Compared with the pristine SnO₂, appropriate Ni doped SnO₂ nanospheres showed much better rate capability and excellent cycling performance. Particularly, the sample with 5 mol% Ni has shown a high initial reversible capacity of 1267 mA h g⁻¹ at a charge-discharge rate of 0.2 C, and a stable reversible capacity of 674.8 mA h g⁻¹ after 35 cycles. Nickel doping could accommodate the huge volume expansion and avoid agglomeration of nanoparticles. Thus, the electrochemistry performance was significantly improved.

Introduction

Lithium-ion batteries, with high reversible capacity, long cycle life, and low cost, have attracted considerable attention in science and industry field.^{1,2,3} Graphite, as the most popular anode material in commercial LIBs anodes, shows excellent cyclability but the low capacity (372 mA h g⁻¹) limits its industrial applications.⁴ In particular, Some promising negative materials such as silicon (Si), tin (Sn), SnO₂, Fe₂O₃, Co₃O₄, and MnO₂ have attracted much interest because of their higher theoretical capacities and higher energy densities than those of conventional graphite anodes.⁵ Among them, tin dioxide (SnO₂), with high theoretical capacity (782 mA h g⁻¹), obtains considerable attention from chemical engineers.⁶ Due to maximum intake of 4.4 Li per Sn atom to form Li_{4.4}Sn during alloying, SnO₂ has been considered as one of the most suitable materials to replace carbon anode in the lithium ion battery. Unfortunately, the practical application of SnO₂-based anodes were hampered by their poor cycling stability. SnO₂ suffers from drastic volume expansion-contraction (~300%) during the Li-ion insertion/extraction reaction and eventually leads to a mechanical failure and loss in electrical activity of the electrode.⁷

To improve the electrochemical performance, significant research efforts have been focused on producing a buffer layer or void space for SnO₂.⁷ These methods include reducing the particle size to nanoscopic dimensions by synthesizing various morphologies of SnO₂, such as zero-dimensional (0D) nanoparticle;⁸ one-dimensional (1D) nanorods, nanobelts,⁹ nanowires and nanotubes;¹⁰ two-dimensional (2D) nanosheet;¹¹ and three-dimensional (3D) hierarchical architectures.¹² For example, Lou et al. reported a one-pot synthesis of SnO₂ hollow nanospheres, which had a high capacity Li-ion storage (about 500

mA h g⁻¹ after 40 cycles at 0.2 C).¹³ Additionally, carbon supported SnO₂ nanocomposites offer an effective way to tailor their electrical and microstructural properties.¹⁴ Lou et al. prepared SnO₂/carbon composite hollow spheres by ternary self-assembly approaches, which displayed a stable reversible capacity about 473 mA h g⁻¹ after 50 cycles.¹⁵ The carbon networks acted as physical buffer for the huge volume change as well as electrical conducting path. There are also efforts to mix SnO₂ with other metal oxides, such as ZnO-SnO₂, CuO-SnO₂, InO₂-SnO₂, SiO₂-SnO₂, NiO-SnO₂.¹⁶⁻¹⁹ Some properties appear in these hybrid systems, such as capability to absorb the volume change and ability to react reversibly with a number of lithium.^{20,21} Due to those properties, the electrochemical performance has been greatly improved.

Nowadays, SnO₂ are also intentionally 'doped' by incorporating atoms or ions of suitable elements into host lattices to enhance cycling stability.^{22,23} For example, Wang et al. synthesized Antimony doped SnO₂ with excellent cycling performance.²⁴ A specific discharge capacity of 637 mA h g⁻¹ was found after 100 cycles at 0.2 C, corresponding to 49.5% of the initial specific capacity.

However, studies on Ni doped SnO₂ as anode materials for lithium-ion batteries have been seldom reported. Herein, we report a simple hydrothermal method for synthesis of Nickel doped SnO₂ nanospheres. Glucose played an important role in mediating the nanospheres. Nickel doping occurred by replacing tin in the crystal structure and the component Ni served as a buffer so that the electrode avoided the usual drastic volume expansion and agglomeration of nanoparticles. Based on this, electrochemical performance of the electrode was significantly improved. Our results indicated the potential applications of Ni doped SnO₂ nanospheres as promising anode material for future

lithium-ion batteries.

Experimental

Preparation of samples

All of the reactants were of analytical grade and used without further purification. The content of Ni was controlled according to the relation: Ni/(Ni + Sn). In a typical synthesis, 0.6 g of tin dichloride dehydrate ($\text{SnCl}_2 \cdot 2\text{H}_2\text{O}$), 2.51 g of sodium citrate ($\text{Na}_3\text{C}_6\text{H}_5\text{O}_7 \cdot 2\text{H}_2\text{O}$) and 5% molar ratio of nickel acetate ($\text{Ni}(\text{CH}_3\text{COO})_2 \cdot 4\text{H}_2\text{O}$) were dispersed in distilled water (15 mL) under stirring. After stirring for several minutes, 0.55 g of glucose was added to solution with continuous stirring to form a transparent solution. Then the solution was transferred into a 25 mL Teflon lined stainless steel autoclave and kept at 180 °C for 9 h. The as-prepared precipitate was separated by centrifugation and washed with distilled water and ethanol for several times. Finally the product was dried at 60 °C overnight. The dried products were annealed at 700 °C under air for 4 h to obtain the SnO_2 nanospheres. For a comparison, the control samples with 0 mol%, 2.5 mol% and 7.5 mol Ni were prepared under identical conditions.

Characterization

XRD measurements were carried out with a Bruker D8 advance X-ray diffractometer with Cu-K α radiation ($\lambda = 0.15418$ nm) in the 2θ range from 20° to 70°. The morphology of as-prepared samples were characterized using a field-emission scanning electron microscope (FE-SEM, Hitachi, S4800) equipped with energy dispersive X-ray spectroscopy (EDS), transmission electron microscope (TEM, JEM 100-CXII, 80 KV) and a high-resolution transmission electron microscope (HRTEM, JEM-2100, 200 kV).

Electrochemical measurement

In order to measure the electrochemical performance of the electrodes, CR2032 coin-type cells were assembled in an argon-filled glove box. The anode electrode was prepared by dispersing 70 wt% active materials, 20 wt% of acetylene black and 10 wt% of Carboxymethyl Cellulose (CMC) binder in distilled water. Then the mixed slurry was spread uniformly on a Cu foil current collector and dried at 90 °C for overnight before testing. The electrolyte was 1 M LiPF₆ in a mixture of ethylene carbonate (EC)-diethyl carbonate (DEC) (1:1 in volume) and the separator was a polypropylene micro-porous film (Cellgard 2400). The charge/discharge tests were performed on a Land CT2001A system (Wuhan, China) at a rate of 0.2 C and in the potential range of 0.005-2.0 V. Cycle voltammograms (CV) curves were recorded on a CHI-630B electrochemical workstation in the range of 0.0-2.50 V (vs. Li+/Li) at the scan rate of 0.2 mV/s. The electrochemical impedance spectroscopy (EIS) was carried out by an electrochemical workstation (MATERIALS MATES 510, ITALIA) by applying an ac in the frequency range of 10 mHz-100 kHz.

Results

Characterization of Ni doped SnO_2 nanospheres

Ni doped SnO_2 nanospheres have been synthesized via one step

hydrothermal method in our work. Their structure and physicochemical properties were investigated via a series of measurement. Fig. 1 shows the XRD patterns for the Ni doped SnO_2 samples and the individual SnO_2 . It indicated all the peaks corresponded to a pure phase (cassiterite, JCPDS No. 41-1445) and no diffraction peaks of crystalline byproducts such as NiO were detected.²⁵ It implied that the nickel doping was constructed by substituting tin in the crystal structure. For the undoped SnO_2 , the peaks at 26.57°, 33.92°, 37.927°, 51.834°, 54.797°, 57.928° and 61.849° were attributed to the (110), (101), (200), (211), (220), (002) and (310)

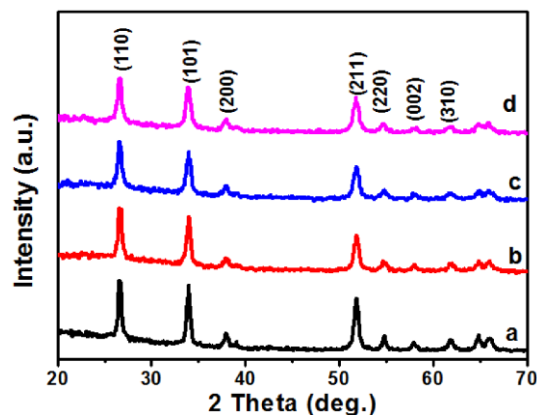


Fig. 1 XRD patterns of (a) pristine SnO_2 , (b) 2.5 mol% Ni- SnO_2 , (c) 5 mol% Ni- SnO_2 , (d) 7.5 mol% Ni- SnO_2

(211), (220), (002) and (310) crystal planes, respectively.

All the samples were also characterized by the Raman spectra, with the exciting laser wavelength of 514 nm, illustrated in Figure 2. For the undoped SnO_2 sample, typical modes positioned at $A_{1g} = 634.7$ cm^{-1} , and $B_{2g} = 778.19$ cm^{-1} were detected.²⁶ Obviously, the strongest typical A_{1g} mode showed a redshift and a decrease of peak intensity with the increase of the Ni^{2+} doping concentration. The main features of the other two bands, labelled as M1 and M2, were associated with surface modes.²⁷ It also could be seen that the peak values dramatically decreased due to the Ni doping. The above phenomena were a powerful evidence of nickel incorporation into the SnO_2 cassiterite lattice.^{27,28} Additionally, no Ni-O

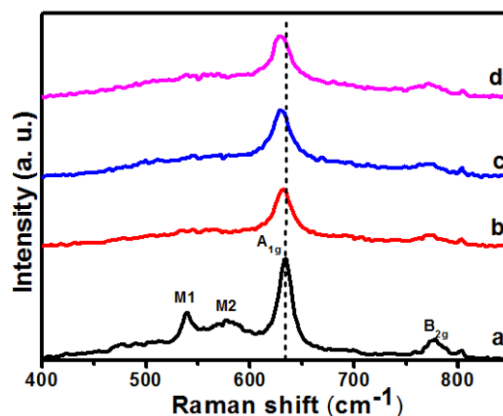


Fig. 2 Raman spectra of (a) pristine SnO_2 , (b) 2.5 mol% Ni- SnO_2 , (c) 5 mol% Ni- SnO_2 , (d) 7.5 mol% Ni- SnO_2

characteristic peak (about 570 cm^{-1}) was detected in the spectrum

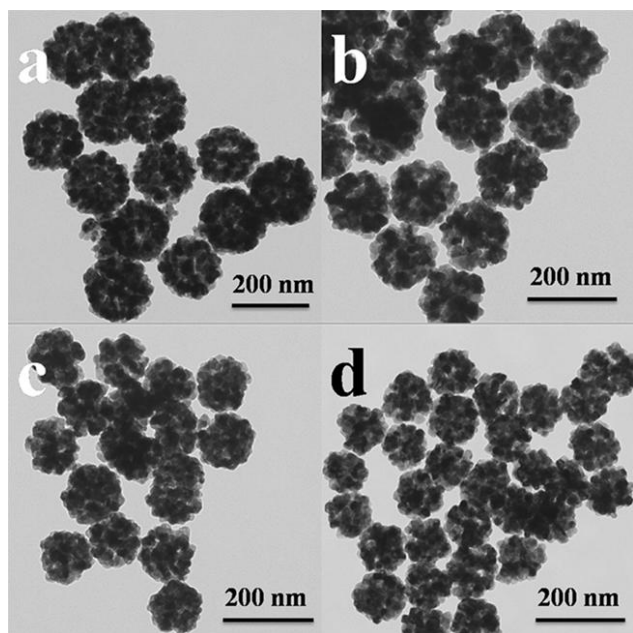


Fig. 3 TEM images of (a) pristine SnO₂, (b) 2.5 mol% Ni-SnO₂, (c) 5 mol% Ni-SnO₂, (d) 7.5 mol% Ni-SnO₂

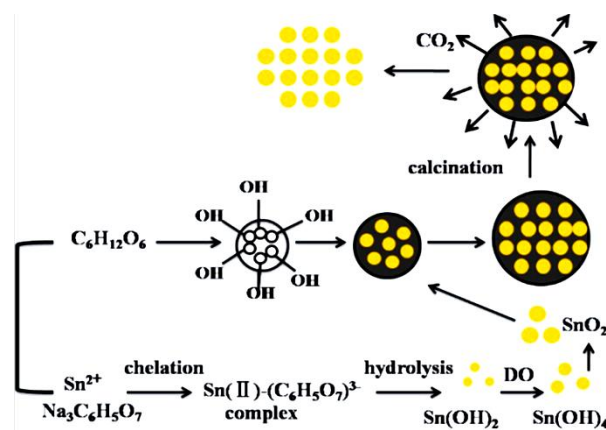
of the doped samples. This was in agreement with the previous XRD results and further confirmed the incorporation of bivalent Ni²⁺ to the SnO₂ cassiterite lattice.

The morphology of the pure SnO₂ and Ni doped SnO₂ samples were examined by TEM and SEM images. Fig. 3 displays the TEM images of the individual SnO₂ and Ni doped SnO₂. All of them were nanospheres composed of numerous tiny nanoparticles. The TEM images also showed that the surface of nanospheres had many pores, indicating good accessibility to the exterior.²² The diameter size of nanospheres for 0 mol% Ni, 2.5 mol% Ni, 5 mol% Ni and 7.5 mol% Ni samples were around 160 nm, 140 nm, 120 nm, 100 nm, respectively. The size of nanospheres slightly reduced with the increasing content of Ni.

The schematic illustration in Scheme 1 was proposed to show the changes during hydrothermal and calcination process. Herein, the introduction of sodium citrate and glucose were important for the preparation of SnO₂ nanospheres. The chelation between divalent tin ions and sodium citrate could efficiently restrain the rapid precipitation of Sn(OH)₂ via hydrothermal treatment, which was beneficial to the oxidation of bivalent tin to tetravalent tin with oxygen dissolved in the solution.²⁹ Besides, glucose was found to play an important role in mediating the spherical structure. The hydrolysis of SnCl₂ occurred in the microenvironment of glucose dehydration and carbon nanospheres loaded with SnO₂ nanoparticles were formed in the hydrothermal reaction.³⁰ After calcination in air, the carbon in the nanospheres was removed, leaving behind the nanospheres structure.

For further investigation on the morphology of nanospheres, the representative SEM image accompanied with EDS spectrum of 5 mol% Ni sample were depicted in Fig. 4a-4b. The nanospheres showed uniform size and good dispersion (Fig. 4a). The EDS spectrum on the nanospheres confirmed the existence of Sn, O and Ni, from which the atom ratio of Ni/(Sn+Ni) was calculated to be 5.09 mol%. Combining the Raman spectrum

analysis, Ni²⁺ has been successfully incorporated into the SnO₂ lattice. The crystal structures and edges of 5 mol% Ni doped SnO₂ were determined with HRTEM (Fig. 4c-4d). Clear lattice fringes were detected in the image. An interplanar spacing of about 0.325 nm corresponded to the (110) planes of SnO₂ and the other one about 0.26 nm was attributed to the (101) planes. Additionally, the selected-area electron diffraction (SAED) pattern (Fig. 4e) of Ni



Scheme 1. Schematic illustration of hydrothermal and calcination process

doped nanospheres showed the characteristic diffraction rings, which was assigned to the (110), (101), (200) and (211) crystal planes. These data were in agreement with the XRD results and indicated the polycrystalline nature of the powder.

Electrochemical performance of Ni doped SnO₂

Fig. 5 exemplifies the discharge cycling performance of different electrodes at 0.2 C in a voltage window of 0.005-2.0 V for 35 cycles. The initial reversible capacity of 954.1 mA h g⁻¹ and the specific discharge capacity of 296.9 mA h g⁻¹ after 35 cycles for pristine SnO₂ were measured. Because of the large volume change during the charge-discharge process, the capacity of SnO₂ decayed rapidly.⁷ In this work, the cycling performance of the SnO₂ enhanced largely with the appropriate content of nickel doping. For example, after 35 cycles, the reversible capacities for 2.5 mol%, 5 mol% and 7.5 mol% Ni doped samples were 230.2 mA h g⁻¹, 674.8 mA h g⁻¹ and 447.8 mA h g⁻¹, respectively. It was found that appropriate molar rate of Ni led to much improved electrochemical performance.

The 5 mol% Ni doped SnO₂ electrode exhibited much better rate capability than the individual SnO₂ at various rates of 0.1 C, 0.2 C, 0.5 C and 1 C (Fig. 6). As shown in Fig. 6, at a rate of 1 C, the specific capacity of 5 mol% Ni doped SnO₂ was about 485.5 mA h g⁻¹ and this was much higher than that of pure SnO₂ electrode (181.9 mA h g⁻¹). When the rate was returned to 0.1 C, the discharge capacity was recovered to 628.9 mA h g⁻¹. The excellent capacity retention was mainly attributed to excellent structural stability. The nickel doping could decrease the lattice volume expansion effect in the alloying and dealloying process. when bivalent nickel substituted tetravalent tin in the crystal structure, Ni was thought to be a buffer for lattice expansion so that it could relief the mechanical stress induced by the large volume change.¹⁹

To further understand the electrochemical process, the cycle

voltammogram (CV) curves of different electrodes for first two cycles were analyzed in Fig. 7. The CV curves (Fig. 7b) of 5 mol% Ni doped SnO₂ were in good agreement with the characteristic of

pristine SnO₂ (Fig. 7a). It was evident that the doping of Ni did not change the electrochemical reaction process. Fig. 7b clearly indicated a strong irreversible reduction peak

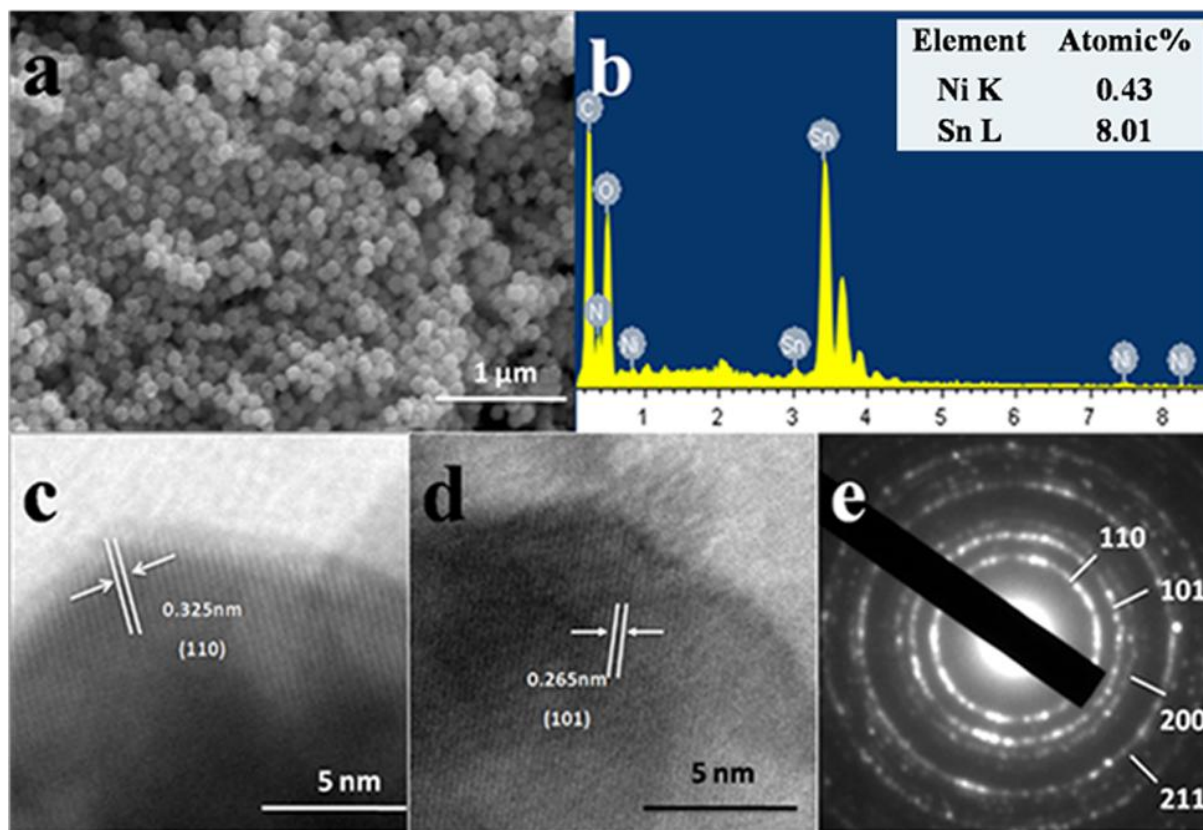


Fig. 4 SEM image (a), EDS spectrum (b), HR-TEM image (c) and (d), corresponding SAED pattern (e) of the as-prepared 5 mol% Ni doped sample

around 0.7 V during the first cycle, which was due to the irreversible reduction of SnO₂ to Sn (Eq. (1)).^{22,24} In the subsequent cycles, this peak would no longer appear.



The irreversible capacity loss during the initial cycles was mostly due to the formation of Li₂O or solid electrolyte interface (SEI) layers.³³ In the first cycle, the cathodic peak at about 0.06 V

as described in Eq. (2).³²



An oxidation peak around 1.3 V and a reduction peak around 0.87 V were assigned to the partially reversible of Eq. (1).³³ This implied that the overall Li storage capacity in SnO₂ anodes increased.³⁴ Compared to pure SnO₂ (Fig. 7a), the potential difference (ΔE) between anodic and cathodic peaks of 5

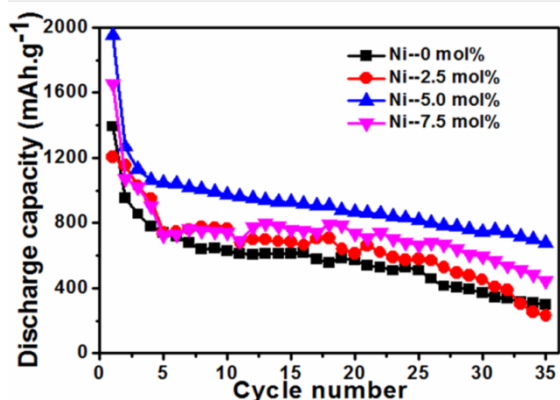


Fig. 5 Cycling performance of SnO₂ and Ni doped SnO₂ samples in the voltage range of 0.005-2.0 V

and the anodic peak at 0.59 V were detected, which were corresponding to the reversible alloying and dealloying (Fig. 7b),

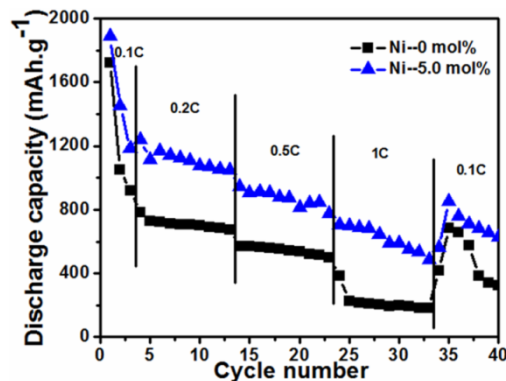


Fig. 6 Rate performance of SnO₂ and 5 mol% Ni doped SnO₂ samples in the voltage range of 0.005-2.0 V.

mol% Ni doped SnO₂ (Fig. 7b) was reduced. The doping of Ni prevented SnO₂ from cracking and led to the improvement of redox behaviour.

Fig. 8 displays the first three voltage profiles for SnO₂ and 5 mol% Ni doped SnO₂ electrodes at a constant current density of 0.2 C. The initial discharge and charge capacity of the Ni doped

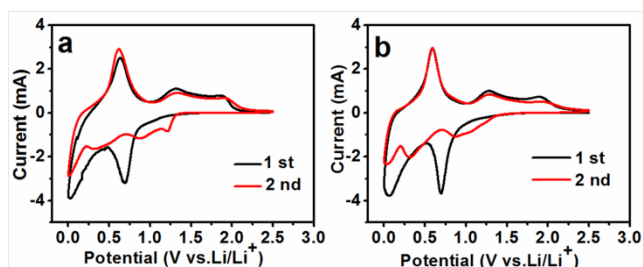


Fig. 7 First second CV curves of SnO₂ and Ni doped SnO₂ anodes: (a) pristine SnO₂, (b) 5 mol% Ni doped SnO₂

anode were much larger than the tin oxide anode. The first discharge capacity for SnO₂ and Ni doped SnO₂ were 1392 mA h g⁻¹ and 1951 mA h g⁻¹, showing a coulombic efficiency of 67.3% and 62.6%, respectively. During the second cycle, the discharge capacity of undoped and doped electrodes decreased to 954 mA h g⁻¹ and 1267 mA h g⁻¹, leading to a much higher coulombic efficiency of 85.2% and 88.9%, respectively. After first cycle, 5 mol% doped sample displayed higher coulombic efficiency than that of individual SnO₂. It was also evident that both of the

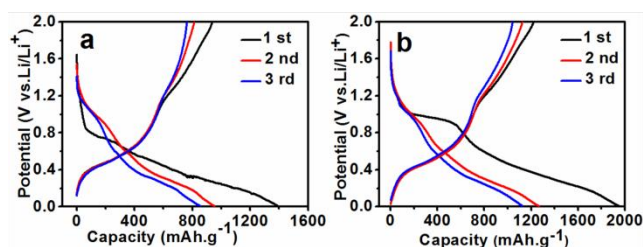


Fig. 8 The initial three charge and discharge curves of (a) pure SnO₂ electrode, (b) the 5 mol% Ni doped electrode.

electrodes exhibited large capacity loss in the subsequent cycles, which was owing to the formation of solid electrolyte interface (SEI) layer and the irreversible reduction of SnO₂ to Sn (Eq. (1)).

To better demonstrate improved electrochemical performance of 5 mol% Ni doped SnO₂, Nyquist plots of the Ni doped and pure SnO₂ were shown in Fig. 9. Before EIS measurement, the electrodes were cycled between 0 and 2.0 V at a 0.1 C rate for 3 cycles and stand for 10 h at 2.0 V to ensure the formation of the stable SEI films on the surface of the electroactive particles. All the electrodes exhibited Nyquist plots composing of a small intercept at high frequency, a circular arc at high to medium frequency and a straight line at low frequency. For Li-ion battery, the intercept in high-frequency region was attributed to ohmic resistance, which represented the total resistance of the electrolyte, separator, and electrical contacts, the circular arc in medium-frequency region was assigned to the charge-transfer impedance on electrode, and the inclined line was corresponding to the lithium-diffusion process within electrodes.^{35,36} The ohmic resistance was similar for all electrodes because the electrodes were prepared by adding a conductive carbon black agent, which meant good conductivity in the electrode. From Fig. 9, it was obvious that for different circular arc, the order of the curvature from small to large was 0 mol%, 2.5 mol%, 7.5 mol% and 5 mol%, respectively. The 5 mol% Ni

doped electrode provided the largest curvature compared with that of others. It indicated that the charge transfer resistance at the electrode/electrolyte interface of the 5 mol% Ni doped SnO₂ was lowest, which consequently decreased the overall battery internal resistance. As a result, the 5 mol% Ni electrode could accordingly have higher reactivity and lower polarization. Based on the above analysis of the tests, the nickel doping was beneficial to enhance the electrochemistry performance.

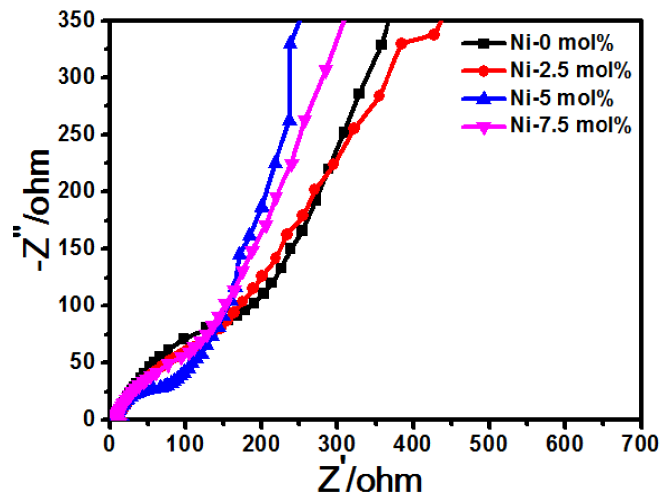


Fig. 9 Electrochemical impedance spectroscopy plots of SnO₂ and Ni doped SnO₂ samples

Conclusions

In summary, using a quite facile hydrothermal route, we have succeeded in fabrication of Ni doped SnO₂ nanospheres with different molar ratios of Ni. In this process, the structure were mediated by glucose. Our work focused on the sample with suitable amount of nickel doping, which exhibited much better cyclic performance and rate capability than the pristine SnO₂. In particular, the sample with 5 mol% Ni had the best electrochemical performance with a high initial reversible capacity of 1267 mA h g⁻¹ at a charge-discharge rate of 0.2 C and a reversible capacity of 674.8 mA h g⁻¹ after 35 cycles. The doping of Nickel acted as a buffer by reducing the volume expansion effect. In addition, the decreasing possibility of tin aggregation during alloying and dealloying process led to lower charge transfer resistance, which brought about overall higher ionic conductivity. It is anticipated that nickel doped SnO₂ nanostructures are an important indication for the further improvement of lithium-ion battery anode of SnO₂-based materials.

Acknowledgments

This study was supported by the Natural Science Foundation of China (Grant 21276142).

Notes and references

- ^a Key Laboratory for Special Functional Aggregate Materials of Education Ministry, School of Chemistry and Chemical Engineering, Shandong University, Jinan 250100, P. R. China.
Tel: +86-531-88365431; Fax: +86-531-88564464;
E-mail address: weihuiying@sdu.edu.cn.

- † Electronic Supplementary Information (ESI) available: See DOI: 10.1039/b000000x/
- 1 S. Ding, J. S. Chen, X. W. Lou, *Adv. Funct. Mater.*, 2011, **21**, 4120.
 - 2 S. P. Wang, H. X. Yang, L. J. Feng, S. M. Sun, J. X. Guo, Y. Z. Yang, H. Y. Wei, *Journal of Power Sources*, 2013, 233, 43. 75
 - 3 W. J. Zhang, Q. J. Liu, L. J. Feng, S. P. Wang, Y. Z. Yang and H. Y. Wei, *New journal of chemistry*, 2014, 38, 2265.
 - 4 S. Ding, D. Luan, F. Y. C. Boey, J. S. Chen, X. W. Lou, *Chem. Commun.*, 2011, 47, 7155. 80
 - 5 C. M. Wang, W. Xu, J. Liu, J. G. Zhang, L. V. Saraf and B. W. Arey, *NanoLett.*, 2011, 11, 1874.
 - 6 C. Wang, Y. Zhou, M. Ge, X. Xu, Z. Zhang and J. Jiang, *J. Am. Chem. Soc.*, 2010, 132, 46.
 - 7 P. G. Bruce, B. Scrosati and J. M. Tarascon, *Angew. Chem. Int. Ed.*, 2008, 47, 2930. 15
 - 8 D. F. Zhang, L. D. Sun, J. L. Yin, C. H. Yan, *Adv. Mater.*, 2003, 15, 1022.
 - 9 J. Z. Wang, N. Du, H. Zhang, J. X. Yu and D. Yang, *J. Phys. Chem. C*, 2011, 115, 11302.
 - 10 Y. Wang, H. C. Zeng, J. Y. Lee, *Adv. Mater.*, 2006, 18, 645.
 - 11 Y. M. Li, X. J. Lv, J. Lu and J. H. Li, *J. Phys. Chem. C*, 2010, 114, 21770.
 - 12 H. Wang, Y. M. Wu, Y. S. Bai, W. Zhou, Y. R. An, J. H. Li and L. Guo, *J. Mater. Chem.*, 2011, 21, 10189.
 - 13 X. W. Lou, Y. Wang, C. Yuan, J. Y. Lee, L. A. Archer, *Adv. Mater.*, 2006, 18, 2325. 25
 - 14 X. W. Lou, J. S. Chen, P. Chen, and L. A. Archer, *Chemistry of Materials*, 2009, 21, 2868.
 - 15 X. W. Lou, D. Deng, J. Y. Lee and L. A. Archer, *Chem. Mater.*, 2008, 20, 5656. 30
 - 16 P. Sun, L. You, Y. Sun, N. Chen, X. Li, H. Sun, J. Ma, G. Lu, *CrystEngComm.*, 2012, 14, 1701.
 - 17 C. Li, W. Wei, S. Fang, H. Wang, Y. Zhang, Y. Gui and R. Chen, *J. Power Sources*, 2010, 195, 2939.
 - 18 H. B. Wu, J. S. Chen, H. H. Hng and X. W. D. Lou, *Nanoscale*, 2012, 4, 2526. 35
 - 19 J. S. Chen and X. W. Lou, *Small*, 2013, 9, 1877.
 - 20 P. Lavela and J. L. Tirado, *J. Power Sources*, 2007, 172, 379.
 - 21 P. Lavela, J. L. Tirado and C. Vidal-Abarca, *Electrochim. Acta*, 2007, 52, 7986. 40
 - 22 Y. D. Wang, T. Chen, *Electrochimica Acta*, 2009, 54, 3510.
 - 23 H. El-Shinawi, M. B. Thm, T. Leichtweiß, K. Peppeler, J. Janek, *Electrochemistry Communications*, 2013, 36, 33.
 - 24 Y. D. Wang, I. Djerdj, B. Smarsly, M. Antonietti, *Chem. Mater.*, 2009, 21, 3202. 45
 - 25 M. F. Hassan, M. M. Rahman, Z. P. Guo, Z. X. Chen and H. K. Li, *J. Mater. Chem.*, 2010, 20, 9707.
 - 26 J. Hays, A. Punnoose, R. Baldner, M. H. Engelhard, J. Peloquin, K. M. Reddy, *Physical Review B*, 2005, 72, 075203.
 - 27 F. H. Aragón, J. A. H. Coaquira, P. Hidalgo, S. W. da Silva, S. L. M. Brito, D. Gouvêa, P. C. Morais, *J. Raman Spectrosc.*, 2011, 42, 1081. 50
 - 28 X. F. Liu, J. Iqbal, Z. B. Wu, B. He, R. H. Yu, *J. Phys. Chem. C*, 2010, 114, 4790.
 - 29 R. Yang, Y. G. Gu, Y. Q. Li, J. Zheng, X. G. Li, *Acta Materialia*, 2010, 9, 864. 55
 - 30 D. Deng, J. Y. Lee, *Chem. Mater.*, 2008, 20, 1841
 - 31 D. Fattakhova, L. Kavan, P. Krtil, *J. Solid State Electrochem.*, 2001, 5, 196.
 - 32 I. A. Courtney, W. R. McKinnon and J. R. Dahna, *Journal of the Electrochemical Society*, 1999, 59, 146. 60
 - 33 Y. Idota, T. Kubota, A. Matsufuji, Y. Maekawa, T. Miyasaka, *Science*, 1997, 276, 1395.
 - 34 Y. S. Lin, J. G. Duh, M. H. Hung, *J. Phys. Chem. C*, 2010, 114, 13136.
 - 35 M. M. Liu, X. W. Li, H. Ming, J. Adkins, X. M. Zhao, L. Su, Q. Zhou and J. W. Zheng, *New J. Chem.*, 2013, 37, 2096. 65
 - 36 Q. J. Liu, F. Yang, S. P. Wang, L. J. Feng, W. J. Zhang, H. Y. Wei, *Electrochimica Acta*, 2013, 111, 903.